

A discrete element simulation of a punch-through shear test to investigate the confining pressure effects on the shear behaviour of concrete cracks

Alireza Bagher Shemirani¹, Vahab Sarfarazi², Hadi Haeri^{*3}, Mohammad Fatehi Marji⁴
and Seyed shahin Hosseini⁵

¹Department of Civil Engineering, Sadra Institute of Higher Education, Tehran

²Department of Mining Engineering, Hamedan University of Technology, Hamedan

³Young Researchers and Elite Club, Bafgh Branch, Islamic Azad University, Bafgh, Iran

⁴Head of Mine Exploitation Engineering Department, Faculty of Mining and Metallurgy, Institution of Engineering, Yazd University, Yazd, Iran

⁵Department of Civil Engineering, Aria University of Sciences and Sustainability, Tehran, Iran

(Received August 12, 2017, Revised October 18, 2017, Accepted October 27, 2017)

Abstract. A discrete element approach is used to investigate the effects of confining stress on the shear behaviour of joint's bridge area. A punch-through shear test is used to model the concrete cracks under different shear and confining stresses. Assuming a plane strain condition, special rectangular models are prepared with dimension of 75 mm×100 mm. Within the specimen model and near its four corners, four equally spaced vertical notches of the same depths are provided so that the central portion of the model remains intact. The lengths of notches are 35 mm. and these models are sequentially subjected to different confining pressures ranging from 2.5 to 15 MPa. The axial load is applied to the punch through the central portion of the model. This testing and models show that the failure process is mostly governed by the confining pressure. The shear strengths of the specimens are related to the fracture pattern and failure mechanism of the discontinuities. The shear behaviour of discontinuities is related to the number of induced shear bands which are increased by increasing the confining pressure while the cracks propagation lengths are decreased. The failure stress and the crack initiation stress both are increased due to confining pressure increase. As a whole, the mechanisms of brittle shear failure changes to that of the progressive failure by increasing the confining pressure.

Keywords: punch-through shear test; confining pressure; shear and tensile cracks; discrete element method

1. Introduction

The mechanical behaviour of rock and concrete structures can be governed by the compression and shear behaviours of the discontinuities and non-persistent cracks existing or induced in these structures as they are subjected to different loading conditions (Einstein 1983, Wong 1998). The influence of crack geometry and mechanical treatment of the non-consistent cracks on the stability analyses of engineering structures are commonly studied by laboratory tests (Yang 2012, Sahouryeh 2002, Baud 1996, Lajtai 1974, Wong 2009, Bobet 1998, Tang 2001, Chen 2013, De Bremaecker 2014).

Many researches have been accomplished to study the cracks initiation, propagation and coalescence in the cracked specimens containing a few open flaws under uniaxial, biaxial and shear loading (Brown 1970, Zhu *et al.* 1997, Bobet and Einstein 1998, Vasarhelyi and Bobet 2000, Wong *et al.* 2001, 2009a, 2009b, Sagong and Bobet 2002, Prudencio 2007, 2009, Ozcebe 2011, Yang *et al.* 2011, Zhou *et al.* 2013, Yin *et al.* 2014, Noël and Soudki 2014, Liu *et al.* 2015, Tiang *et al.* 2015, Wan Ibrahim *et al.* 2015, Yang 2015, Silva *et al.* 2015, Gerges *et al.* 2015, Haeri *et al.*

2013, Haeri *et al.* 2015a, Haeri 2015b, Li *et al.* 2015, Li *et al.* 2016, Li *et al.* 2016, Haeri and Sarfarazi 2016a, 2016b, 2016c, Haeri *et al.* 2016d, Sarfarazi *et al.* 2016b, Sarfarazi 2016a, 2016b, Sardemir 2016, Wang *et al.* 2017). In the most of these laboratory tests, it is difficult to measure the failure mechanism of bridge area (intact material in between the rock joints) during the loading process. However, the numerical simulations of these tests are good alternatives to investigate the failure behaviour and fracturing mechanism of these non-persistent cracks using techniques such as the finite element method, displacement discontinuity method, dual boundary element method, discrete element method, and hybridized method (Chan 1990, Bobet 2001, Tang 2000, Tang 2000a, 200b, Zhang 2009, Mughieda 2009). Among these simulations approach the discrete element method (DEM) originally proposed by Cundall and Stark since 1979 is appropriate to model most of the experimental tests and study the mechanical behaviors of soils and rocks for rock engineering applications. In the particle flow codes, the materials are envisioned as an assembly of elements in the form of arbitrary circular disks (in 2D case) or spherical particles (in 3D case) which are programmed in the PFC2D and PFC3D, respectively. The pioneers in providing a realistic calibration procedure for micro-mechanical parameters of PFC3D for a contact bonded particle model were Kulatilake *et al.* (2001). A cracked rock model was also established in their analyses using the effect of closed

*Corresponding author, Assistant Professor
E-mail: h.haeri@bafgh-iau.ac.ir, haerihadi@gmail.com

flaws. They also studied the mechanical behaviour of the cracked rock model under uniaxial loading condition and established a relation between micro-parameters and macro parameters. The open flaws have been created in the bonded particle model by removing some of the particles at the specified location (Ghazvinian 2012, Sarfarazi 2014).

The crack propagation process is studied for one, two and three open flaws by Zhang (2011), Zhang and Wong (2013). Most of the modelled crack propagation patterns obtained by the numerical works are quite similar to those observed in the laboratory tests. The smooth-crack model is another way to model the mechanical behaviour of a crack in PFC program. The smooth-crack model proposed by Bahaaddini *et al.* (2013) is used in a bonded particle program to study the influence of cracks geometry on the fracturing mechanism of the non-persistent jointed rock mass.

In the present research, the specimens designed for a Punch Through Shear (PTS) tests have been modelled by a discrete element code to study the shear behaviour of the non-persistent cracks under different confining pressure. The laboratory Brazilian test results are being used to measure the micromechanical parameters of concrete specimen used in the numerical simulation. The inverse modelling calibration approach is used to validate the shear behaviour of the bridge area estimated by the numerical modelling. These results are compared with those measured by the PTS tests in the laboratory. The calibrated modelling samples are used to continue the investigation into the shear behaviour of the pre-cracked models under different confining pressures.

2. Numerical modelling of the problem

The discrete element modelling is used to investigate the effects of sample shapes on their tensile strength and I_s (50). A two dimensional particle flow code which employs a bonded particle model is appropriate for the numerical modelling.

2.1 The discrete element modelling

A particle flow computer code based on the discrete element method is used for the numerical analyses of the mechanical problems involving the movement of disc particles within a confined body. A group of particles with a uniform size-distribution are created so that these assemblies have radii in the range of the minimum radius to the maximum radius of the particles. It is then possible to create particles with different shapes so that each particle assembly acts as an autonomous object. Each assembly is assumed to form a bonded particle model which should satisfy the following assumptions. 1) each individual particle is a rigid body; 2) The particle contacts occur over a small area (point); 3) these contacts are established to obey the soft-contact approach behaviour; 4) at the contact points (areas) all the (rigid) particles overlap; 5) the induced force assigns the magnitude of these overlaps (which are small compared to the particle sizes); 6) all the contact points are bonded to each other.

The contact and parallel bonds are the two mostly used bonding behaviours in between the discs. The normal and shear contact forces are considered as zero when the bonds break i.e., when the tensile normal contact force exceeds the normal contact bond strength. If the shear force does not exceed the friction (at equilibrium conditions) and the normal force is compressive and does not altered, the bonds may break in shear, when the shear contact force equals or exceeds the shear contact bond strength.

In the present research a parallel bond model is used to model the micro-mechanical behaviour of a brittle rock-like material. As shown in Table 1, the parallel bond approach includes eight micro-mechanical parameters (of the specified body) which are related to the macro-mechanical behaviour of the intact material. Some equations are being used in the discrete element approach but as far as the calibrating of the micromechanical parameters is concerned no solid theory can calibrate these parameters with the experimentally measured micromechanical properties of the material. Therefore, this calibration is usually carried out through a trial and error procedure. However, in general, the normal and shear strengths of the bond and its elastic modulus are related to those of the modelled particle.

2.2 Preparing and calibrating the numerical model used for the analyses

Generally, four main steps are involved in preparing a test model in a standard discrete element code such as PFC2D. These steps may be regarded as: (a) generating and packing process of the particles is established, (b) an isotropic state of stress is specified, (c) the floating particles are eliminated, and (d) the bonded particle models are installed.

The tensile strength of the bonded model in discrete element analyses can be calibrated via Brazilian tensile test results. The standard calibration procedure (three calibrated particle assembly) as adopted from Cundall and Dark (1979) are considered (the micro-properties listed in Table 1). The Brazilian discs of 54 mm in diameter are modelled in the numerical modelling tests. These disc specimens

Table 1 The material's micro-properties used to represent the model with a tensile strength of 4.6 MPa

Property	Value	Property	Value
Type of particle	disc	Parallel bond radius multiplier	1.4
Density (kg/m ³)	2000	Youngs modulus of parallel bond (GPa)	40
Minimum radius (mm)	0.27	Parallel bond stiffness ratio	1.7
Size ratio	1.56	Particle friction coefficient	0.4
Porosity ratio	0.08	Parallel normal strength, mean (MPa)	25
Local damping coefficient	0.7	Parallel normal strength, std. dev (MPa)	2
Contact young modulus (GPa)	4	Parallel shear strength, mean (MPa)	25
Stiffness ratio (kn/ks)	1.7	Parallel shear strength, std. dev (MPa)	2

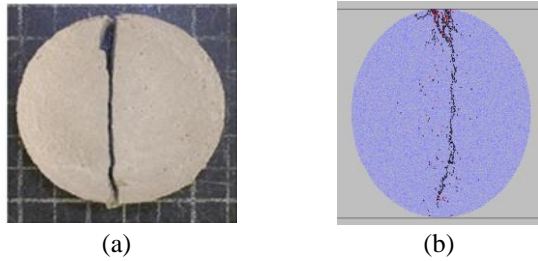


Fig. 1 The tensile fracturing patterns of Brazilian disc samples in (a) numerical model, (b) experimental specimens

were tested by allowing the lateral walls move toward each other at a low speed of 0.016 m/s. The failure processes of the tested specimens for the numerical and experimental tests are illustrated in Fig. 1(a) and Fig. 1(b), respectively. These Figures show that there is a good matching in between the failure planes experienced in numerical and laboratory tests. The numerical and experimental values of the tensile tests are 4.2 MPa and 4 MPa, respectively, which are close to each other too and therefore the numerical results are validated.

2.3 The numerical simulation of punch through shear test samples with non-persistent open cracks

The shears through tests on the pre-cracked samples are numerically simulated by the discrete element code after its calibration. Fig. 2 shows a proposed shear box model (with dimension of 75×100 mm.) to simulate this problem (Fig. 2). The shear box model samples are discretized by 11,179 circular disc elements with a minimum radius of 0.27 mm. The two non-persistent vertical bands of particles are deleted from the banded particles model to create the planar non-persistent cracks already existing in the original experimental test specimens. Then in the upper and lower parts of the models, four vertical (parallel) notches with equal lengths of 35 mm are made with the horizontal distance 40 mm and bridge length 30 mm. (Fig. 2). The influence of confining pressure on the shear behaviour of bridge areas is investigated by simulating six specimens each containing edge-notched cracks with similar lengths. For each of these simulated models, seven different confining pressures (i.e., 2.5, 3.5, 4.5, 7, 9, 12 and 15 MPa. are selected to study the individual models.

2.4 Set up for the shear loading devices

Loading of the model is performed by setting up the five loading walls (Fig. 2). Various confining pressures are applied to the model by moving (turning) the loading walls $id=1$ and $id=2$ in the positive side (counter clockwise) and negative side (clockwise) of x -axis, respectively.

The shear loadings are applied to the model (sample) by moving the lower wall in the positive Y -axis and the upper wall in the opposite direction of the Y -axis slowly (with an adequate low velocity of 0.016 m/s) to ensure a quasi-static equilibrium conditions. The normal stress is kept constant by adjusting the velocity of the left and right walls by a numerical servo-control mechanism. The shear

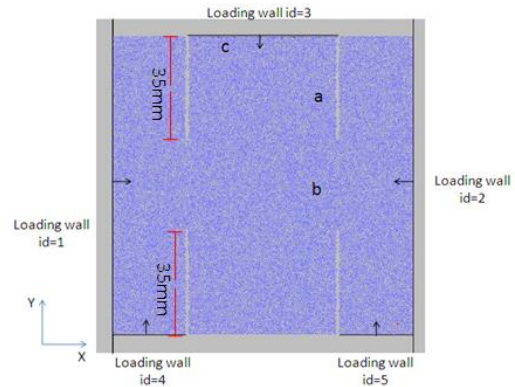


Fig. 2 A specified model for the punch-through shear test

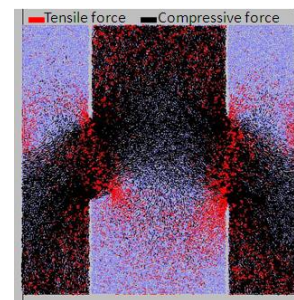


Fig. 3 The parallel bond force distribution vectors before the crack initiation process in the modelled samples under a confining pressure of 2.5 MPa

displacement is measured by tracing the upper wall displacement (i.e., wall 3 as shown in Fig. 2). The corresponding shear force is also registered by taking the reaction forces on the wall 3.

3. The distribution of force and displacement vectors in the modelled samples

The numerical model of the punch through shear test gives the distribution of force and displacement in the model during the loading time. During the process of cracks initiation, propagation and failure of the numerical models the vectors of displacements and loads distribution within different parts of the samples can be visualized.

3.1 The modelled parallel bond forces before the crack initiation process

The parallel bond force distribution (as shown in Fig. 3) illustrates the state of force vectors within the modelled samples before the crack initiation process under a confining pressure of 2.5 MPa. The red and dark lines shown in Fig. 3 represent the tensile and compression force vectors in the model, respectively. The coarse lines and their accumulation show the areas where larger forces are induced within the model. It can be easily seen that the tensile forces of the bonded particles at the tip of the crack are less than their shear strength, therefore, the tensile crack initiation is a dominant mode of fracturing that initiates at the tip of the crack within the modelled samples.

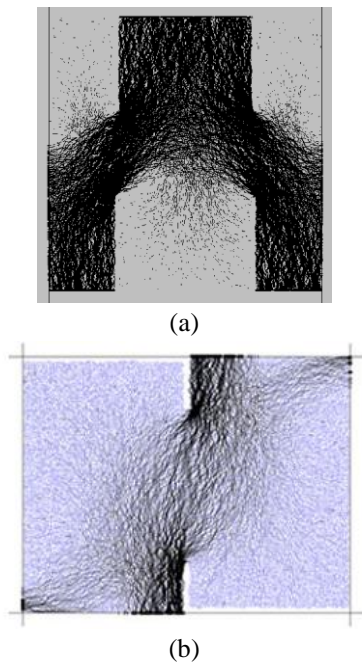


Fig. 4 (a) the contact force distribution before the crack initiation process in the model under a confining pressure of 2.5 MPa, (b) a typical contact force distribution in a pre-cracked model under a direct shear loading as reported by Ghazvinian *et al.* (2012)

3.2 The modelled contact forces before the crack initiation

The contact force vectors shown in Fig. 4(a) illustrate the contact force distribution under the confining pressure of 2.5 MPa before the crack initiation process. Fig. 4(b) shows a typical contact force distribution in a pre-cracked model under a direct shear loading as reported by Ghazvinian *et al.* (2012). The black lines are parallel to the contact forces, and their thicknesses are proportional to the magnitude of these forces. As shown in these figures, the contact forces in the modelled samples are not uniformly distributed as the sample approaches its peak strength. In the pre-cracked models, the contact forces are concentrated near the crack tips due to the crack initiation in the intact material model. However, in both samples, the contact forces in the centre of the sample are inclined to the direction of shearing by approximately 0° - 40° .

3.3 The distribution of displacement vectors in the modeled samples

The distribution of particle displacement vectors in the modelled sample under a confining pressure of 2.5 MPa is shown in Fig. 5(a). The typical displacement vector observed in the Brazilian tensile test simulation using the same micro-parameters as in the punch through shear test is shown in Fig. 5(b). The displacement vectors of the particles in a modelled sample illustrate how the particles are moving as they are subjected to the external loading conditions. Fig. 5 illustrates that in both the direct shear test and the Brazilian test, the displacement vectors show

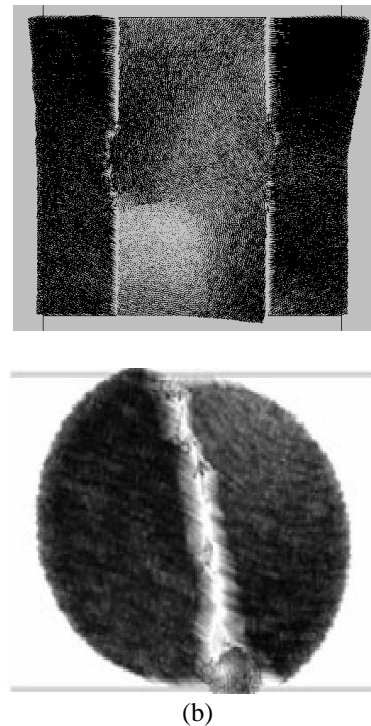


Fig. 5 (a) The particle displacement vectors in the modelled samples under confining pressure of 2.5 MPa, (b) The displacement vectors observed in a Brazilian tensile test

similar trends, and the fractures display a tensile mode of failure, characteristic of Mode I fractures (the fracture mechanics terminology for fractures subjected to tensile loading conditions).

4. The effects of confining pressure on the failure behavior of the modelled samples

The micromechanical behaviour and fracture patterns of the modelled samples with the planar non-persistent cracks under various confining pressures (2.5, 3.5, 4.5, 7, 9, 12 and 15 MPa) are considered to study the effects of confining pressure on fracturing process of the brittle materials in a punch through shear test.

4.1 Failure mechanism of the model at a confining pressure of 2.5 MPa

In the failure mechanism of the modelled samples at a confining pressure of 2.5 MPa, the tensile wing cracks may initiate from the crack tips and propagate diagonally with respect to the direction of shear loading. Fig. 6(a) shows several shear bands developed within the bridge area and led to the spalling failure of the specimen. As shown in the shear loading diagram of Fig. 6(b), the bridge area may exhibit a linear elastic behaviour at the beginning of shear loading then, as the loading increases, this behaviour gradually changes to that of non-linear. However, from the results shown in Fig. 6(c), it can be concluded that cracks initiates at shear loading of 877 KN., where 475 tensile micro-cracks are developed with in the model while the

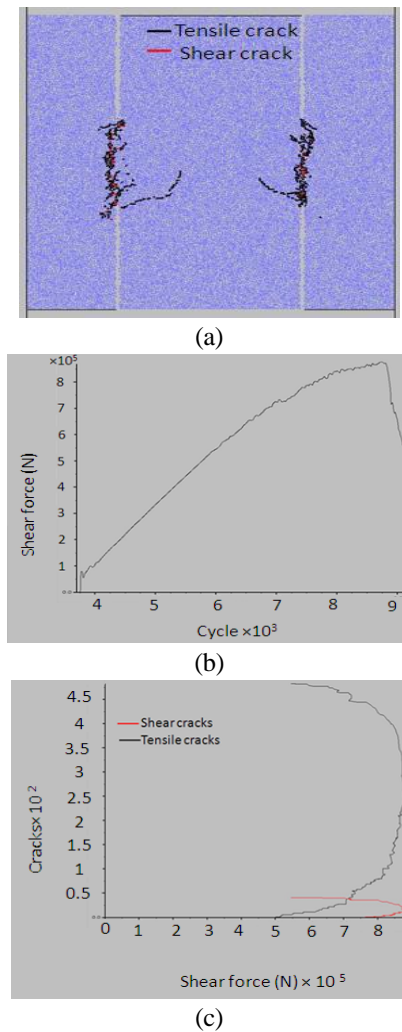


Fig. 6 (a) The fracture patterns of non-persistent crack in the modelled samples for a confining pressure of 2.5 MPa, b) The shear force versus the cycle, (c) The variation of cracks number versus the applied force

number of shear cracks reaches to 35. Due to the lower tensile strength of the modelled samples the tensile cracks are the most dominant mode of failure compared to those of shear mode. At the peak shear loading condition, a total number of 250 tensile cracks are developed while the number of shear cracks reaches to 13.

4.2 Failure mechanism of the model at a confining pressure of 3.5 MPa

The tensile wing cracks initiates from the crack tips at a confining pressure is 3.5 MPa. These cracks propagate diagonally with respect to the direction of shear loading condition. Fig. 7(a) shows several shear bands that are developed within the bridge area and cause the spalling failure of the sample. However, Fig. 7(b) shows the shear loading diagram that the bridge area may have a linear elastic behaviour at the beginning of the shear loading which gradually changes to that of non-linear as the loading increases. Fig. 7(c), illustrates that the cracks may initiate at the shear loading of 975 KN., where, 527 tensile cracks are

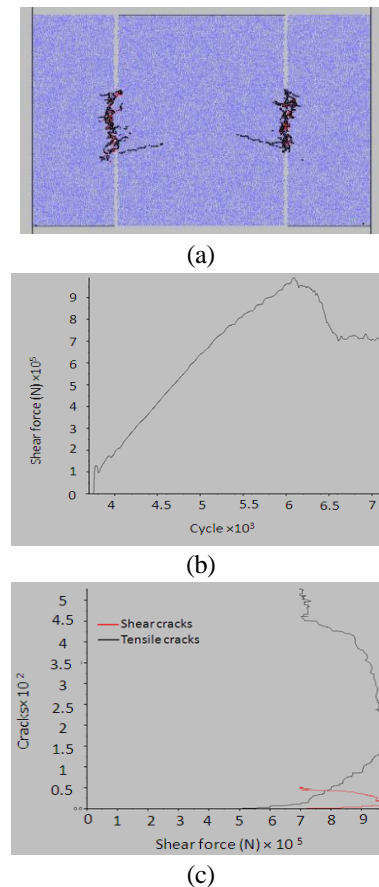


Fig. 7 (a) the fracture patterns of the non-persistent cracks in the samples with a confining pressure of 3.5 MPa, (b) the shear force versus the cycle, (c) the variation of cracks number versus the applied force

developing within the modelled sample while the number of shear cracks is only 46. In this case again the tensile cracks are the dominant mode of failure in the model. It should be noted that 190 tensile cracks are developed at the peak shear loading conditions while at the same conditions the shear cracks number is only 10.

4.3 Failure mechanism of the model at a confining pressure of 4.5 MPa

Fig. 8(a) shows several shear bands developed within the bridge area of the joints and cause the spalling of the specimen at a confining pressure of 4.5 MPa. While the shear loading diagram shown in Fig. 8(b) illustrates that the intact material within the bridge area has a linear elastic behaviour at the beginning of shear loading but this behaviour changes to that of non-linear one with increase in the loading. However, as shown in Fig. 8(c), it can be easily concluded that the tensile and shear cracks initiate at shear loading of 992 KN. A total number of 552 tensile cracks are developed within the modelled samples while the number of shear cracks increase to 75. Therefore, the tensile cracks are the dominant mode of failure that occurs in the modelled samples. It's to be noted that about 150 tensile cracks are developed at the peak shear loading condition while the number of shear cracks is around 10 at this stage.

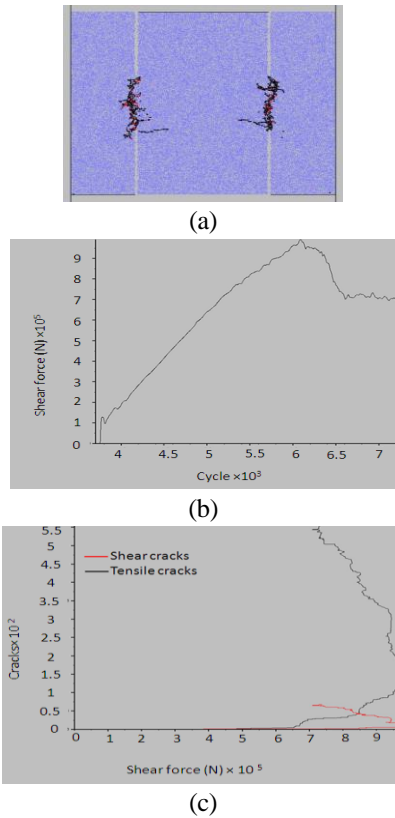


Fig. 8 (a) The fracture patterns of the non-persistent cracks in the modelled samples under a confining pressure of 4.5 MPa, (b) The shear force versus the (loading)cycle, (c) The cracks number versus the applied force

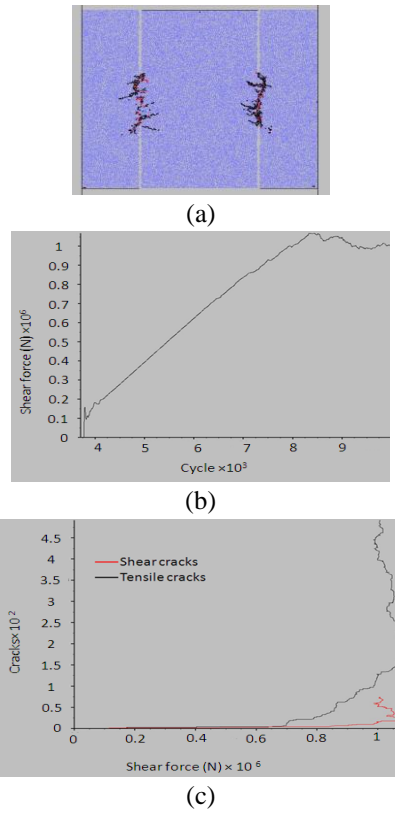


Fig. 9 (a) the fracture patterns of non-persistent crack in the modelled samples at a confining pressure of 7 MPa, (b) The shear force versus The cycle, (c) the cracks number versus the applied force

4.4 Failure mechanism of the model at a confining pressure of 7 MPa

As shown in Fig. 9(a), several shear bands may have developed within the bridge area and cause the spalling failure of the modelled specimens. This figure illustrates that the number of wing cracks decreases with an increase in the confining pressure. Fig. 9(b) shows the shear loading diagram which illustrate that the bridge area (i.e., the intact part of the specimen) has a linear elastic behaviour at the beginning of shear loading while this behaviour changes to that of non-linear one with an increase in the loading. From the results shown in Fig. 9(c), it can be concluded that the tensile and shear cracks initiate at a shear loading of 1069 KN. The number of tensile cracks within the modelled samples is about 475 while that of the shear cracks is about 75 under shear loading condition. The tensile cracks are again the dominant mode of failure that occur in the modelled samples because a total number of 200 tensile cracks are developed at peak shear loading while the number of shear cracks reaches to 20 at this stage.

4.5 Failure mechanism of the model at a confining pressure of 9 MPa

Fig. 10(a) shows that as the confining pressure reaches to 9 MPa, again several shear bands are developed within the bridge area of the modelled samples and spalling failure

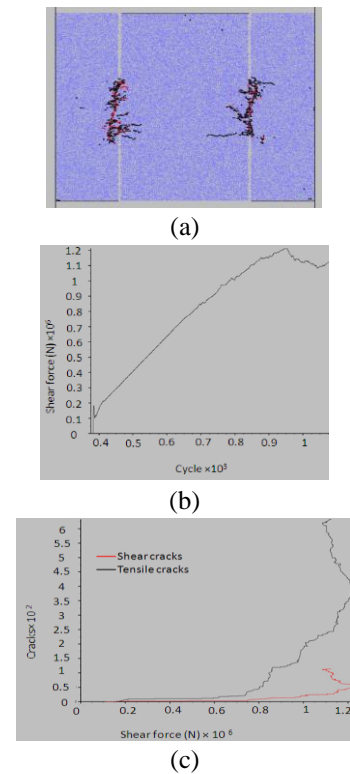


Fig. 10 (a) the fracture patterns of the non-persistent cracks of the models for a confining pressure of 9 MPa, (b) The shear force versus the cycle, (c) The cracks number versus the applied force

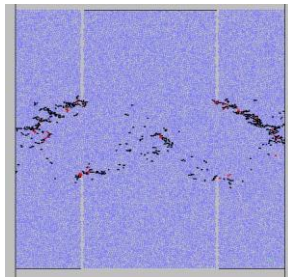


Fig. 11 The fracture patterns of the modelled samples with non-persistent cracks for a confining pressure of 12 MPa

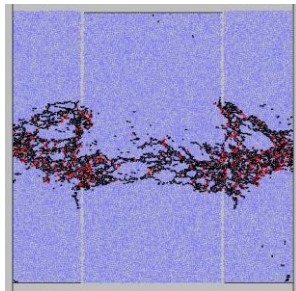


Fig. 12 The fracture patterns of the models with non-persistent cracks for a confining pressure of 15 MPa

of the specimen is occurred. This figure again validates that as the confining pressure increases the number of wing cracks decreases. The shear loading diagram of Fig. 10(b) illustrates that the bridge area within the model has a linear elastic behaviour at the beginning of shear loading and changes to that of non-linear as the loading increases. From the results shown in Fig. 10(c), it may be concluded that the tensile and shear cracks initiate at shear loading of 1069 KN. The total number of tensile cracks developed within the model reaches to 656 while those of shear cracks are about 110. This case is also like the previous cases and shows that the tensile cracks are the most dominant mode of failure and a total number of 375 tensile cracks are developed at the peak shear loading while those of shear cracks reaches to 55 at this stage.

4.6 Failure mechanism of the model at confining pressures of 12 MPa and 15 MPa

Finally, Figs. 11 and 12 illustrate the tensile failure of the modelled samples at confining pressures of 12 MPa and 15MPa, respectively. These Figures again validates that as the confining pressure increases the number of wing cracks decreases and tensile failure dominants that of shear in the modelled samples.

5. The effect of confining pressure on the failure stress and crack initiation stress

The variations of failure stresses and the crack initiation stresses versus the confining pressure are depicted graphically in Fig. 13. Both of these stresses are increasing as the confining pressure is increased. However, as shown in the graphs, the failure stresses increase more than those

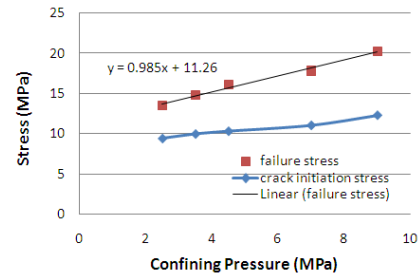


Fig. 13 Variation of the failure stresses and crack initiation stresses versus the confining pressure

of the crack initiation.

own in Fig. 13, the relation between the peak of failure stress and the confining pressure is a linear fitting curve while that of the peak shear load is also almost linear but with a smaller slope to the confining pressure. However, from the fitting equations under high confining pressure, $y=0.985x+11.26$ for the case of failure stress analysis. It may be concluded that the peak of shear stress is 11.26 MPa. for the specimens with no confining pressure.

6. Discussions

In the present work, the punch through shear test specimens are modelled numerically by the discrete element method and their shearing behaviours under various confining pressure is studied. Firstly, the micromechanical parameters of concrete cracks used in the numerical simulation are measured experimentally by the laboratory Brazilian test results to calibrate the numerical modelling technic. Secondly, the shear behaviour of the pre-cracked modelled samples under various confining pressure is investigated numerically.

Comparing the results shown in Figs. 6-13, one may conclude that the capacity of the bridge area to resist the shear loading has a close relationship with the failure mechanism of the modelled samples. By increasing the confining pressure, the shear band numbers and the peak shearing load are increased and usually in most cases the tensile fracture failure is the most dominant fracturing mode of the modelled samples compared to that of the shear cracks mode of loading.

As shown in Fig. 13, for the confining pressure of 2.5 MPa, the brittle concrete failure mechanism is dominant because the difference between the failure stress and the crack initiation stress is small (fracture mechanics principles). On the other hand, when the confining pressure is high (for example 9 MPa in Fig. 13), the difference between the failure stress and the crack initiation stress is high enough to cause a progressive concrete fracturing failure mechanism based on the fracture mechanics principles. This means that the brittle failure mechanism changes to that of the progressive failure by increasing the normal load at the specified confining pressures. For the case of pre-cracked specimens, it may be concluded that the peak of shear load is mostly influenced by its fracture pattern, while the fracture pattern of the bridge area is mainly controlled by the confining pressure.

7. Conclusions

A discrete element modelling approach is used to simulate the effect of confining pressure on the shear behaviour of concrete cracks modelled in a punch through shear test. In the modelled samples, four equally spaced vertical notches are provided at equal distance from the four specimen corners. The length of each individual notch is 35 mm. The modelled samples are subjected to different confining pressures (ranging from 2.5 to 15 MPa). Then, the central portion of the modelled sample is compressed axially.

Some of the basic conclusions may be counted as the following.

- The total number of the shear cracks produced in the modelled samples is increases as the confining pressure increases.
- At the low confining pressure (2.5 MPa), failure of the modelled specimens is mainly governed by the induced tensile load.
- At the higher confining pressures, the effects of shear stresses increase so that the mixed shear/tensile stresses are basically responsible for the bond breakage in the bonded modelled samples.
- The number of shear bands and their mean orientations are increased by increasing the confining pressure but their propagation lengths are decreased.
- As the confining pressure increases the symmetrical failure surface changes to that of the non-symmetrical rough surface and a stable crack growth may occur in the samples.
- The shear band number and the capacity of bridge area within the modelled samples (to resist the shear loading) are increased by increasing the confining pressure.
- The increase in the confining pressure also increases the crack initiation stress and the failure stress.
- At a low confining pressure (2.9 MPa) as shown in Fig. 12(a), the brittle failure as defined in concrete mechanics context is occurred because the difference between the failure stress and crack initiation stress is small.
- At a higher confining pressure (9 MPa) as shown in Fig. 12(b), the progressive fracturing failure (crack propagation phenomenon) as defined in concrete fracture mechanics context is occurred.
- It is concluded that when the confining pressure is three times of the tensile strength of the modelled samples, their failure dominantly control by the confining pressure.

References

- Bahaaddini, M., Sharrock, G. and Hebblewhite, B.K. (2013), "Numerical investigation of the effect of joint geometrical parameters on the mechanical properties of a non-persistent jointed rock mass under uniaxial compression", *Comput. Geotech.*, **49**, 206-225.
- Baud, P., Reuschlé, T. and Charlez, P. (1996), "An improved wing crack model for the deformation and failure of rock in compression", *Int. J. Rock Mech. Min. Sci. Geomech. Abs.*, **33**(5), 539-542.
- Bobet, A. (2001), "A hybridized displacement discontinuity method for mixed mode I-II-III loading", *Int. J. Rock Mech. Min. Sci.*, **38**(8), 1121-1134.
- Bobet, A. and Einstein, H.H. (1998), "Fracture coalescence in rock-type materials under uniaxial and biaxial compression", *Int. J. Rock Mech. Min. Sci.*, **35**(7), 863-888.
- Bobet, A. and Einstein, H.H. (1998), "Numerical modeling of fracture coalescence in a model rock material", *Int. J. Fract.*, **92**(3), 221- 252.
- Brown, E.T. (1970), "Strength of models of rock with intermittent joints", *J. Soil Mech. Found. Div.*, ASCE, **96**, 1935-1949.
- Chan, H.C.M., Li, V. and Einstein, H.H. (1990), "A hybridized displacement discontinuity and indirect boundary element method to model fracture propagation", *Int. J. Fract.*, **45**(4), 263-282.
- Chen, X., Liao, Z.H. and Peng, X. (2013), "Cracking process of rock mass models under uniaxial compression", *J. Central South Univ.*, **20**(6), 1661-1678.
- Cundall, P.A. and Strack, O.D.L. (1979), "A discrete numerical model for granular assemblies", *Geotechnique*, **29**(1), 47-65.
- De Bremaecker, J.C. and Ferris, M.C. (2004), "Numerical models of shear fracture propagation", *Eng. Fract. Mech.*, **71**(15), 2161-2178.
- Einstein, H.H., Veneziano, D., Baecher, G.B. and O'Reilly, K.J. (1983), "The effect of discontinuity persistence on rock slope stability", *Int. J. Rock Mech. Min. Sci. Geomech. Abs.*, **20**(5), 227-36.
- Gerges, N., Issa, C. and Fawaz, S. (2015), "Effect of construction joints on the splitting tensile strength of concrete", *Case Stud. Constr. Mater.*, **3**, 83-91.
- Ghazvinian, A., Sarfarazi, V., Schubert, W. and Blumel, M. (2012), "A study of the failure mechanism of planar non-persistent open joints using PFC2D", *Rock Mech. Rock Eng.*, **45**(5), 677-693.
- Haeri, H. (2015), "Influence of the inclined edge notches on the shear-fracture behavior in edge-notched beam specimens", *Comput. Concrete*, **16**, 605-623.
- Haeri, H. and Sarfarazi, V. (2016a), "The effect of micro pore on the characteristics of crack tip plastic zone in concrete", *Comput. Concrete*, **17**(1), 107-12.
- Haeri, H. and Sarfarazi, V. (2016b), "The effect of non-persistent joints on sliding direction of rock slopes", *Comput. Concrete*, **17**(6), 723-737
- Haeri, H. and Sarfarazi, V. (2016c), "The deformable multilaminate for predicting the elasto-plastic behavior of rocks", *Comput. Concrete*, **18**, 201-214.
- Haeri, H., Khaloo, A. and Fatehi Marji, M. (2015), "Fracture analyses of different preholed concrete specimens under compression", *Acta Mech Sin*, **31**(6), 855-870.
- Haeri, H., Sarfarazi, V. and Lazemi, H.A. (2016d), "Experimental study of shear behavior of planar non-persistent joint", *Comput. Concrete*, **17**(5), 639-653.
- Haeri, H., Shahriar, K., Marji, M.F. and Moarefvand, P. (2013), "Modeling the propagation mechanism of two random micro cracks in rock Samples under uniform tensile loading", *13th International Conference on Fracture*, Beijing, China.
- Kulatilake, P.H.S.W., Malama, B. and Wang, J. (2001), "Physical and particle flow modeling of jointed rock block behavior under uniaxial loading", *Int. J. Rock Mech. Min. Sci.*, **38**(5), 641-657.
- Lajtai, E.Z. (1974), "Brittle fracture in compression", *Int. J. Fract.*, **10**(4), 525-536.
- Li, J. Y., Zhou, H., Zhu, W. and Li, S. (2016), "Experimental and numerical investigations on the shear behavior of a jointed rock mass", *Geosci. J.*, **20**, 371-379.
- Li, S., Wang, H., Li, Y., Li, Q., Zhang, B. and Zhu, H. (2016), "A new minigrating absolute displacement measuring system for static and dynamic geomechanical model tests", *Measur.*, **82**,

- 421-431.
- Li, Y., Zhou, H., Zhu, W., Li, S. and Liu, J. (2015), "Numerical study on crack propagation in brittle jointed rock mass influenced by fracture water pressure", *Mater.*, **8**(6), 3364-3376.
- Liu, X., Nie, Z., Wu, S. and Wang, C. (2015), "Self-monitoring application of conductive asphalt concrete under indirect tensile deformation", *Case Stud. Constr. Mater.*, **3**, 70-77.
- Mughieda, O. and Karasneh, I. (2006), "Coalescence of offset rock joints under biaxial loading", *Geotech. Geolog. Eng.*, **24**(4), 985-999.
- Noël, M. and Soudki, K. (2014), "Estimation of the crack width and deformation of FRP-reinforced concrete flexural members with and without transverse shear reinforcement", *Eng. Struct.*, **59**, 393-398.
- Ozcebe, G. (2011), "Minimum flexural reinforcement for T-beams made of higher strength concrete", *Can. J. Civil Eng.*, **26**, 525-534.
- Prudencio, M. (2009), "Study of the strength and failure mode of rock mass with non-persistent joints", Ph.D. Thesis, Catholic University of Chile, Santiago, Chile.
- Prudencio, M. and Van Sint Jan, M. (2007), "Strength and failure modes of rock mass models with non-persistent joints", *Int. J. Rock Mech. Min. Sci.*, **44**(6), 890-902
- Sagong, M. and Bobet, A. (2002), "Coalescence of multiple flaws in a rock-model material in uniaxial compression", *Int. J. Rock Mech. Min. Sci.*, **39**(2), 229-241
- Sahouryeh, E., Dyskin, A.V. and Germanovich, L.N. (2002), "Crack growth under biaxial compression", *Eng. Fract. Mech.*, **69**(18), 2187-2198,
- Sardemir, M. (2016), "Empirical modeling of flexural and splitting tensile strengths of concrete containing fly ash by GEP", *Comput. Concrete*, **17**(4), 489-498.
- Sarfarazi, V. and Haeri, H., (2016a), "Effect of number and configuration of bridges on shear properties of sliding surface", *J. Min. Sci.*, **52**(2), 245-257.
- Sarfarazi, V., Faridi, H.R., Haeri, H. and Schubert, W. (2016b), "A new approach for measurement of anisotropic tensile strength of concrete", *Adv. Concrete Constr.*, **3**(4), 269-284
- Sarfarazi, V., Ghazvinian, A., Schubert, W., Blumel, M. and Nejati, H.R. (2014), "Numerical simulation of the process of fracture of Echelon rock joints", *Rock Mech. Rock Eng.*, **47**(4), 1355-1371.
- Sarfarazi, V., Haeri, H. and Khaloo, A. (2016b), "The effect of non-persistent joints on sliding direction of rock slopes", *Comput. Concrete*, **17**(6), 723-737.
- Silva, R.V., Brito, J. and Dhir, R.K. (2015), "Tensile strength behaviour of recycled aggregate concrete", *Constr. Build. Mater.*, **83**, 108-118.
- Tang, C.A. and Kou, S.Q. (1998), "Crack propagation and coalescence in brittle materials under compression", *Eng. Fract. Mech.*, **61**(3-4), 311-324.
- Tang, C.A., Lin, P., Wong, R.H.C. and Chau, K.T. (2001), "Analysis of crack coalescence in rock-like materials containing three flaws-Part II: numerical approach", *Int. J. Rock Mech. Min. Sci.*, **38**(7), 925-939.
- Tang, C.A., Liu, H., Lee, P.K.K., Tsui, Y. and Tham, L.G. (2000a), "Numerical studies of the influence of microstructure on rock failure in uniaxial compression-art I: Effect of heterogeneity", *Int. J. Rock Mech. Min. Sci.*, **37**(4), 555-569.
- Tang, C.A., Tham, L.G., Lee, P.K.K., Tsui, Y. and Liu, H. (2000b), "Numerical studies of the influence of microstructure on rock failure in uniaxial compression-Part II: constraint, slenderness and size effect", *Int. J. Rock Mech. Min. Sci.*, **37**(4), 571-583.
- Tiang, Y., Shi, S., Jia, K. and Hu, S. (2015), "Mechanical and dynamic properties of high strength concrete modified with lightweight aggregates presaturated polymer emulsion", *Constr. Build. Mater.*, **93**, 1151-1156.
- Vasarhelyi, B. and Bobet, A. (2000), "Modeling of crack initiation, propa-gation and coalescence in uniaxial compression", *Rock Mech. Rock Eng.*, **33**(2), 119-139
- Wan Ibrahim, M.H., Hamzah, A.F., Jamaluddin, N., Ramadhansyah, P.J. and Fadzil, A.M. (2015), "Split tensile strength on self-compacting concrete containing coal bottom ash", *Procedia-Soc. Behav. Sci.*, **198**, 2280-2289.
- Wang, X., Zhu, Z., Wang, M., Ying, P., Zhou, L. and Dong, Y. (2017), "Study of rock dynamic fracture toughness by using VB-SCSC specimens under medium-low speed impacts", *Eng. Fract. Mech.*, **181**, 52-64.
- Wong, L.N.Y. and Einstein, H.H. (2009a), "Crack coalescence in molded gypsum and Carrara marble: part 1. Macroscopic observations and interpretation", *Rock Mech. Rock Eng.*, **42**(3), 475-511
- Wong, L.N.Y. and Einstein, H.H. (2009b), "Systematic evaluation of cracking behavior in specimens containing single flaws under uniaxial compression", *Int. J. Rock Mech. Min. Sci.*, **46**(2), 239-249
- Wong, R.H.C. and Chau, K.T. (1998), "Crack coalescence in a rock-like material containing two cracks", *Int. J. Rock Mech. Min. Sci.*, **35**(2), 147-164.
- Wong, R.H.C. and Einstein, H.H. (2009), "Crack coalescence in molded gypsum and Carrara marble: Part I. macroscopic observations and interpretation", *Rock Mech. Rock Eng.*, **42**(3), 475-511.
- Wong, R.H.C., Chau, K.T., Tang, C.A. and Lin, P. (2001), "Analysis of crack coalescence in rock-like materials containing three flaws-part I: experimental approach", *Int. J. Rock Mech. Min. Sci.*, **38**(7), 909-924
- Yang, S.Q. (2015), "An experimental study on fracture coalescence characteristics of brittle sandstone specimens combined various flaws", *Geomech. Eng.*, **8**, 541-557
- Yang, S.T., Hu, X.Z. and Wu, Z.M. (2011), "Influence of local fracture energy distribution on maximum fracture load of three-point-bending notched concrete beams", *Eng. Fract. Mech.*, **78**, 3289-99.
- Yang, Y.F., Tang, C.A. and Xia, K.W. (2012), "Study on crack curving and branching mechanism in quasibrittle materials under dynamic biaxial loading", *Int. J. Fract.*, **177**(1), 53-72.
- Yin, P., Wong, R.H.C. and Chau, K.T. (2014), "Coalescence of two parallel preexisting surface cracks in granite", *Int. J. Rock Mech. Min. Sci.*, **68**, 66-84
- Zhang, H., He, Y., Han, L., Jiang, B., Liang, Z. and Zhong, S. (2009), "Microfracturing characteristics in brittle material containing structural defects under biaxial loading", *Comput. Mater. Sci.*, **46**(3), 682-686.
- Zhang, X.P. and Wong, L.N.Y. (2011), "Cracking processes in rock-like material containing a single flaw under uniaxial compression: A numerical study based on parallel bonded-particle model approach", *Rock Mech. Rock Eng.*, **45**(5), 711-737.
- Zhang, X.P. and Wong, L.N.Y. (2013), "Crack initiation, propagation and coalescence in rock-like material containing two flaws: a numerical study based on bonded-particle model approach", *Rock Mech. Rock Eng.*, **46**(5), 1001-1021.
- Zhou, X.P., Cheng, H. and Feng, Y.F. (2013), "An experimental study of crack coalescence behaviour in rock-like materials containing multiple flaws under uniaxial compression", *Rock Mech. Rock Eng.*, **47-6**, 1961-1986.
- Zhu, Z., Xie, H. and Ji, S. (1997), "The mixed boundary problems for a mixed mode crack in a finite plate", *Eng. Fract. Mech.*, **6**(5), 647-655.